Thermochromic polymer opals

Jason Sussman,[1] David Snoswell,[1] Andreas Kontogeorgos,[1] Jeremy J. Baumberg,[1,a)] and Peter Spahn[2]

[1]*NanoPhotonics Centre, Cavendish Laboratory, University of Cambridge, Cambridge CB3 OHE, United Kingdom*
[2]*Deutsches Kunststoff-Institut, Schlossgartenstrasse 6, D-64289 Darmstadt, Germany*

Large-scale shear-ordered photonic crystals are shown to exhibit unusual thermochromic properties. By balancing the refractive index of the polymer core and composite shell components at room temperature, transparent films are created, which become colored on heating to 150 °C. Since this scattering-based structural color depends only on resonant Bragg scattering of the unpigmented components, it can be tuned to any wavelength. The observed color shifts with temperature are not simply accounted for by theory and are sensitive to the constituents. © *2009 American Institute of Physics*. [doi:10.1063/1.3256193]

Manmade thermochromic materials fall into two categories. Phase transition thermochromics[1–4] realign their atomic crystal structure on reaching a critical temperature thus changing their color, and are found in products such as disposable battery indicators.[5] Other types (particularly thermochromic liquid crystals) change color continuously, but only within a small ΔT range[6–9] and have been widely used to map surface temperature distributions.[10] Similar results have been reported for metastable gels of block copolymers that form a lamellar phase whose Bragg reflection can be temperature tuned.[11] Neither category describes the material reported here, which shows little color shift but displays a thermally induced continuous change from transparency to spectrally resonant scattering. Such materials are examples of an unconventional class of structural color nanocomposites with tunable properties.

Thermochromic polymer opals are based on the flexible monolithic photonic crystals we have explored recently and are made of hard polymer spheres dispersed in a softer sticky elastomer matrix.[12,13] As typical for opaline photonic crystals,[14–16] when the spheres self-assemble into a fcc lattice they can be color tuned by changing the size of the constituent spheres. Using $\simeq 200$ nm diameter spheres produces Bragg peaks in the visible-IR spectral range, while the elastomeric composition gives flexible films with enhanced structural control of color. A major strength of our work is the ability to form these opals by shear assembly in extrusion or compression which allows efficient production on industrial scales.

Here, polymer opals with striking thermochromic properties are produced by designing sphere and matrix to have equal refractive indices at room temperature, hence Fresnel reflections at the sphere surfaces are suppressed and the film is transparent. As the temperature is increased, these refractive indices change at different rates. The result is increasingly strong resonant Bragg scattering that causes structural color to progressively appear (Fig. 1), an effect that is reversed on cooling and repeats over multiple thermal cycling. This thermochromic mechanism can be harnessed in a wide variety of ways by tuning core and shell sizes and compositions.

Thermochromic polymer opals with $\Delta n=0$ at room temperature ("balanced opals") are produced from monodisperse precursor core/shell spheres comprised of a polymethylmethacrylate (PMMA) core and a composite shell of 70% polyethylacrylate (PEA) and 30% polybenzylmethacrylate, grown using similar methods to our previous core-shell precursors.[17,18] This material is then sheared by being extruded and then pressed (at 150 °C and 1.9 MPa for 5 min). When the polymer opal material is pressed against a flat plate, the shell material fuses into a matrix and the spheres shear assemble into a lattice with the (111) plane parallel to the surface. In previous work,[12,13] we have shown that doping polymer opals with <0.1% by weight of sub-50-nm carbon nanoparticles (which uniformly incorporate in the outer matrix) dramatically enhances the resonant Bragg scattering so that specific colors emerge in a broad scattering cone. The balanced thermochromic samples are compared with our previous versions which have $\Delta n=0.1$ at room temperature ("nonbalanced opals") and consist of a polystyrene inner core and a PEA shell, providing strong structural color at room temperature. We thus contrast four types of samples: with and without refractive index contrast at room temperature, and with and without carbon doping that can enhance structural color.

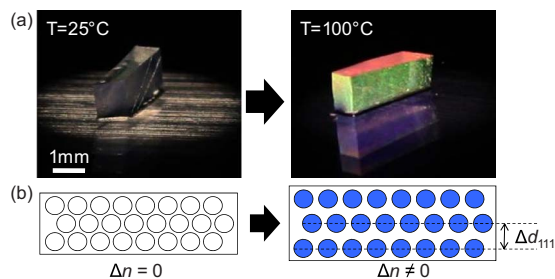We quantify optical scattering spectra of different samples by mounting them on a heated stage and recording

FIG. 1. (Color online) (a) Images of a "balanced" thermochromic polymer opal sample heated from $T=25-100$ °C. (b) Structure of balanced thermochromic opal showing both isotropic expansion with refractive index changes on heating.
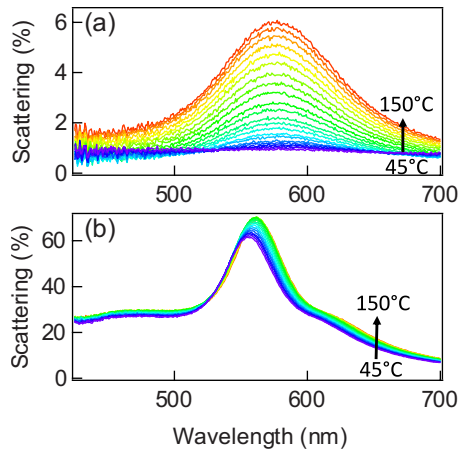
a)Electronic mail: jjb12@cam.ac.uk.

95, 173116-1

FIG. 2. (Color online) Scattering spectra of (a) balanced ($\Delta n = 0$ at $T = 20\ ^\circ$C) and (b) nonbalanced ($\Delta n = 0.1$ at $T = 20\ ^\circ$C) 0.05% carbon-doped polymer opals from $T = 45$ to 150 $^\circ$C in 5 $^\circ$C steps. Spectra are normalized to white diffuser plates.

confocally collected dark-field spectra on a modified microscope. Data is normalized to the scattering spectra taken under identical conditions on white diffuser plates with a broadband Lambertian spectrum. The collected spot diameter at the sample is 10 μm using 20× objectives (numerical aperture=0.45), with light in a dark field configuration incident at 27° and collected at normal incidence ($\theta < 20°$).

Balanced thermochromic samples [Fig. 2(a)] have a weak featureless scattering spectrum at room temperature, but a significant scattering peak emerges around λ_{pk} =580 nm on heating, as refractive index contrast develops between the shell-derived matrix and 220 nm diameter spheres. This reflects the transition from transparent to green color seen in Fig. 1. Similarly, heating a nonbalanced polymer opal to 150 $^\circ$C raises the pre-existing scattering peak by 9% [Fig. 2(b)]. The difference in the resonant linewidth between these two samples originates in the thickness and degree of order of the opal and reflects the nonoptimized shear ordering for the balanced shell composition. However, it is clear that in both materials, increasing reflection at each sphere interface creates an unusual type of thermochromic effect, which is limited in temperature range only by the decomposition temperatures of the constituent polymers.

In all cases, the scattering increases quadratically with temperature [Fig. 3(a)], both for the balanced ($\Delta n = 0$) and nonbalanced ($\Delta n = 0.1$) opals. This accords with a simple theory presented below. Carbon doping affects both scattered intensity and λ_{pk}, with the addition of carbon nanoparticles in all cases leading to extra absorption reducing the scattered light emerging. Examining the spectra at $T = 150\ ^\circ$C [Fig. 3(b)] shows a surprising increase in Bragg wavelength, λ_{pk}, on adding carbon nanoparticles implying that despite the low levels of loading and undisrupted lattice, the average lattice spacing increases. This effect is also seen in the original nonbalanced opals, and may arise because the nanoparticles modify the rheology during the shear-ordering process.[19]

Extracting the peak scattering λ_{pk} as temperature increases reveals a wide range of behaviors [Fig. 3(c)]. Resonant Bragg scattering is controlled by the condition λ_{pk} = $2\bar{n}d_{111}\sin\theta$, where $\bar{n}$ is the volume-weighted average refractive index. While thermal expansion *increases* the lattice
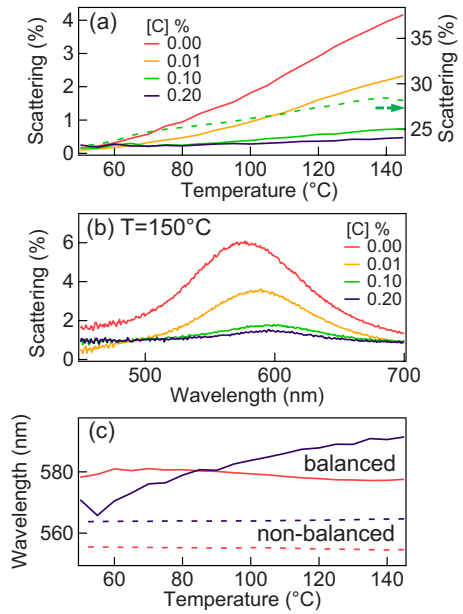

FIG. 3. (Color online) (a) Normalized scattering spectra of balanced thermochromic polymer opals at 150 $^\circ$C and (b) peak scattering strength vs temperature, for samples with increasing carbon nanoparticle doping up to 0.2% by weight. Dashed line shows nonbalanced opal (right axis); dotted line shows quadratic fit to scattering vs temperature. (c) Peak scattered wavelength vs temperature for balanced (solid) and nonbalanced samples (dashed), both with (blue) and without (red) carbon nanoparticle doping.

spacing, it *reduces* the refractive index, leading to competing control over λ_{pk}. The glass transition temperature of PEA is 0 $^\circ$C and of PMMA is 110 $^\circ$C, hence the heavily crosslinked PMMA has an expansivity (κ_s) less than a third of that of PEA (κ_m) in this temperature range.[20] Thermogravimetric analysis shows no sign of PMMA or PEA decomposition below 180 $^\circ$C, and no degradation of the films is observed at 150 $^\circ$C although rheological properties will be different. For small temperature changes ΔT,

$$\Delta f = f(1-f)(\kappa_s - \kappa_m)\Delta T, \tag{1}$$

$$\Delta d_{111} = \left(\frac{2g+1}{3}\right)\bar{\kappa}\Delta T d_{111}, \tag{2}$$

where the sphere fill fraction $f = 0.55$ and the volume-averaged expansivity $\bar{\kappa} = f\kappa_c + (1-f)\kappa_s$. The extent to which the film is allowed to expand laterally as compared to vertically is parameterized by g, which is 0 for isotropic expansion and 1 for vertical expansion only (film pinned laterally to the substrate).

As the material expands, its optical density falls according to the Clausius–Mossotti equation,[21] which with Eq. (1) yields for the dielectric constant in each medium

$$\epsilon(T + \Delta T) = \epsilon(T) - \kappa\Delta T[\epsilon(T) - 1][\epsilon(T) + 2]/3, \tag{3}$$

$$\Delta\bar{n} \simeq -\bar{\kappa}\Delta T(\bar{n}^2 - 1)(\bar{n}^2 + 2)/(6\bar{n}), \tag{4}$$

where $\Delta\bar{n}$ is the thermally induced change in refractive index contrast. For small refractive index contrasts between matrix and spheres in balanced opals,

$$\frac{\Delta\lambda_{pk}}{\lambda_{pk}} = \frac{\Delta\bar{n}}{\bar{n}} + \frac{\Delta d_{111}}{d_{111}} \simeq \bar{\kappa}\Delta T\left(\frac{2g}{3} - 0.055\right). \qquad (5)$$

As $\bar{\kappa} \simeq 4.8 \times 10^{-4}$ K^{-1},[20] the wavelength shift should lie between 3.0% and -0.3% for $\Delta T = 100$ K. Figure 3(c) shows redshifts up to 5.6% and blueshifts up to 0.15%, which are largely accounted for by different sample constraints on the expansion. But the model does not expain the significant dependence on carbon nanoparticle loading, nor the nonlinear behavior of the wavelength shift. One likely origin of this failure is the way the current model assumes that strain is uniformly spatially distributed within this heterogeneous nanocomposite, when local compression and relaxation are possible.

Despite these anomalies, this simple model predicts a quadratic temperature-dependent increase in optical scattering strength [c.f. Fig. 3(a)]. While the reflected intensity at each sphere-matrix interface increases as Δn^2, optical scattering is proportional to $[\Delta\epsilon/(\epsilon_s + 2\epsilon_m)]^2$.[22] We thus predict that the maximum scattering $S_{max} \propto \Delta\kappa\Delta T^2$ independent of the original refractive index contrast, in good agreement with our data at small temperature rises.

The spectral linewidth of the Bragg peaks is unaffected by temperature, remaining 50 nm in these thermochromic opals independent of the carbon loading. Since the Bragg linewidth is mainly a function of the disorder and not the index contrast, this confirms structural electron microscopy that carbon nanoparticles do not affect the basic internal opal structure,[13] even if they slightly affect the spacing between spheres. This is also confirmed in our one-dimensional distributed feedback reflector model, in which the linewidth increases little with refractive index contrast despite increased optical penetration through the structure.[19,23]

In summary, we demonstrate a thermochromic material with scattering strength increasing continuously with increasing temperature, but without strong color shifts. Balanced thermochromic opals are transparent at room temperature and their colors appear not because of a change in material phase, but because of a temperature-dependent change in refraction. Emerging refractive index contrast produces structural color, with wavelength shifts that can be tuned by modifying the composition and cross-linking of the sphere and matrix polymers. Simultaneous changes in reflectivity and transmission are weaker in these opals, due to the structural color mechanism[12] and the internal disorder. Further optimization and incorporation of other (e.g., emissive) nanoparticles thus open a range of potential applications in sensing, displays, and structural color materials.

[1] A. Seeboth, J. Kriwanek, and R. Vetter, Adv. Mater. **12**, 1424 (2000).
[2] S. Kubo, Z. Gu, K. Takahashi, A. Fujishima, H. Segawa, and O. Sato, J. Am. Chem. Soc. **126**, 8314 (2004).
[3] L. Liu, S. Peng, W. Wen, and P. Sheng, Appl. Phys. Lett. **90**, 213508 (2007).
[4] M. Ibisate, D. Golmayo, C. Lopez, and J. Opt, Pure Appl. Opt. **10**, 125202 (2008).
[5] J. F. Hughen, U.S. Patent No. 5,612,151 (18 March 1997).
[6] K. Yoshino, Y. Manda, K. Sawada, M. Onoda, and R. Sugimoto, Solid State Commun. **69**, 143 (1989).
[7] M. Seredyuk, A. Gaspar, V. Ksenofontov, S. Reiman, Y. Galyametdinov, W. Haase, E. Renschler, and P. Gutlich, Chem. Mater. **18**, 2513 (2006).
[8] J. M. Leger, A. L. Holt, and S. A. Carter, Appl. Phys. Lett. **88**, 111901 (2006).
[9] M. Harun-ur-Rashid, T. Seki, and Y. Takeoka, Chem. Rec. **9**, 87 (2009).
[10] C. R. Smith, D. R. Sabatino, and T. J. Praisner, Exp. Fluids **30**, 190 (2001).
[11] J. Yoon, W. Lee, and E. L. Thomas, Macromolecules **41**, 4582 (2008).
[12] O. L. J. Pursiainen, J. J. Baumberg, H. Winkler, B. Viel, P. Spahn, and T. Ruhl, Opt. Express **15**, 9553 (2007).
[13] O. L. J. Pursiainen, J. J. Baumberg, H. Winkler, B. Viel, P. Spahn, and T. Ruhl, Adv. Mater. **20**, 1484 (2008).
[14] Y. Vlasov, V. Astratov, A. Baryshev, A. Kaplyanskii, O. Karimov, and M. Limonov, Phys. Rev. E **61**, 5784 (2000).
[15] S. Romanov, T. Maka, C. Sotomayor Torres, M. Muller, R. Zentel, D. Cassagne, J. Manzanares-Martinez, and C. Jouanin, Phys. Rev. E **63**, 056603 (2001).
[16] M. McLachlan, N. Johnson, R. De La Rue, and D. McComb, J. Mater. Chem. **14**, 144 (2004).
[17] T. Ruhl, P. Spahn, and G. P. Hellmann, Polymer **44**, 7625 (2003).
[18] T. Ruhl, P. Spahn, H. Winkler, and G. P. Hellmann, Macromol. Chem. Phys. **205**, 1385 (2004).
[19] D. Snoswell, A. Kontogeorgos, J. J. Baumberg, T. D. Lord, M. R. Mackley, P. Spahn, and G. P. Hellmann (unpublished).
[20] D. W. Van Krevelen, *Properties of Polymers* (Elsevier, Amsterdam, 1990).
[21] D. J. Griffiths, *Introduction to Electrodynamics*, 3rd ed. (Prentice-Hall, Upper Saddle River, 1999).
[22] C. F. Bohren and D. R. Huffman, *Absorption and Scattering of Light by Small Particles* (Wiley-Interscience, New York, 1998).
[23] A. Kavokin, J. J. Baumberg, G. Malpuech, and F. P. Laussy, *Microcavities* (Oxford University Press, Oxford, 2008).